Acta Crystallographica Section D
Biological Crystallography
ISSN 1399-0047

Structure and mechanism of a nonhaem-iron SAM-dependent *C*-methyltransferase and its engineering to a hydratase and an *O*-methyltransferase

Xiao-Wei Zou,[a]‡ Yu-Chen Liu,[a,b,c]‡ Ning-Shian Hsu,[a] Chuen-Jiuan Huang,[a] Syue-Yi Lyu,[a] Hsiu-Chien Chan,[a] Chin-Yuan Chang,[a] Hsien-Wei Yeh,[a] Kuan-Hung Lin,[a] Chang-Jer Wu,[d] Ming-Daw Tsai[b,c,e] and Tsung-Lin Li[a,b,f]*

[a]Genomics Research Center, Academia Sinica, Taipei 115, Taiwan, [b]Chemical Biology and Molecular Biophysics Program, Taiwan International Graduate Program, Institute of Biological Chemistry, Academia Sinica, Taipei 115, Taiwan, [c]Institute of Biochemical Sciences, National Taiwan University, Taipei 115, Taiwan, [d]Department of Food Science, National Taiwan Ocean University, Keelung 202, Taiwan, [e]Institute of Biological Chemistry, Academia Sinica, Taipei 115, Taiwan, and [f]Biotechnology Center, National Chung Hsing University, Taichung 402, Taiwan

‡ These authors contributed equally.

Correspondence e-mail: tlli@gate.sinica.edu.tw

Received 6 January 2014
Accepted 6 March 2014

PDB references: SeMppJ–SAH–MePpy, 4kib; MppJ–SAM–Ppy, 4kic; MppJ–Ppy, 4kif; MppJ–4HPpy, 4kig; MppJ D244E, 4m6x; MppJ D244L, 4m6y; MppJ R127L/D244E, 4m71; MppJ R127L/V300E, 4m72; MppJ R127L/D244A/V300E, 4m73; MppJ (SAH/Ppy) R127L/D244A/V300E, 4m74

In biological systems, methylation is most commonly performed by methyltransferases (MTs) using the electrophilic methyl source *S*-adenosyl-L-methionine (SAM) *via* the S_N2 mechanism. (2*S*,3*S*)-β-Methylphenylalanine, a nonproteinogenic amino acid, is a building unit of the glycopeptide antibiotic mannopeptimycin. The gene product of *mppJ* from the mannopeptimycin-biosynthetic gene cluster is the MT that methylates the benzylic C atom of phenylpyruvate (Ppy) to give βMePpy. Although the benzylic C atom of Ppy is acidic, how its nucleophilicity is further enhanced to become an acceptor for *C*-methylation has not conclusively been determined. Here, a structural approach is used to address the mechanism of MppJ and to engineer it for new functions. The purified MppJ displays a turquoise colour, implying the presence of a metal ion. The crystal structures reveal MppJ to be the first ferric ion SAM-dependent MT. An additional four structures of binary and ternary complexes illustrate the molecular mechanism for the metal ion-dependent methyltransfer reaction. Overall, MppJ has a nonhaem iron centre that bind, orients and activates the α-ketoacid substrate and has developed a sandwiched bi-water device to avoid the formation of the unwanted reactive oxo-iron(IV) species during the *C*-methylation reaction. This discovery further prompted the conversion of the MT into a structurally/functionally unrelated new enzyme. Through stepwise mutagenesis and manipulation of coordination chemistry, MppJ was engineered to perform both Lewis acid-assisted hydration and/or *O*-methyltransfer reactions to give stereospecific new compounds. This process was validated by six crystal structures. The results reported in this study will facilitate the development and design of new biocatalysts for difficult-to-synthesize biochemicals.

1. Introduction

The *S*-adenosyl-L-methionine (SAM)-dependent methyltransferases (MTs) represent one of the most diverse and biologically important classes of enzymes (Fontecave *et al.*, 2004). These enzymes utilize the ubiquitous SAM as the methyl donor to methylate a wide variety of biomolecules such as nucleic acids, proteins, lipids and primary and secondary metabolites (Schubert *et al.*, 2003; Martin & McMillan, 2002). (2*S*,3*S*)-β-Methylphenylalanine (βMePhe), a nonproteinogenic amino acid, is a building unit of mannopeptimycin (Fig. 1*a*; He *et al.*, 2002) and some other secondary metabolites (Houge-Frydrych *et al.*, 2000). Mannopeptimycin is a hopeful drug lead, the biosynthetic gene cluster for which (*mpp*) has recently been identified (Magarvey *et al.*, 2006). The *mppJ*

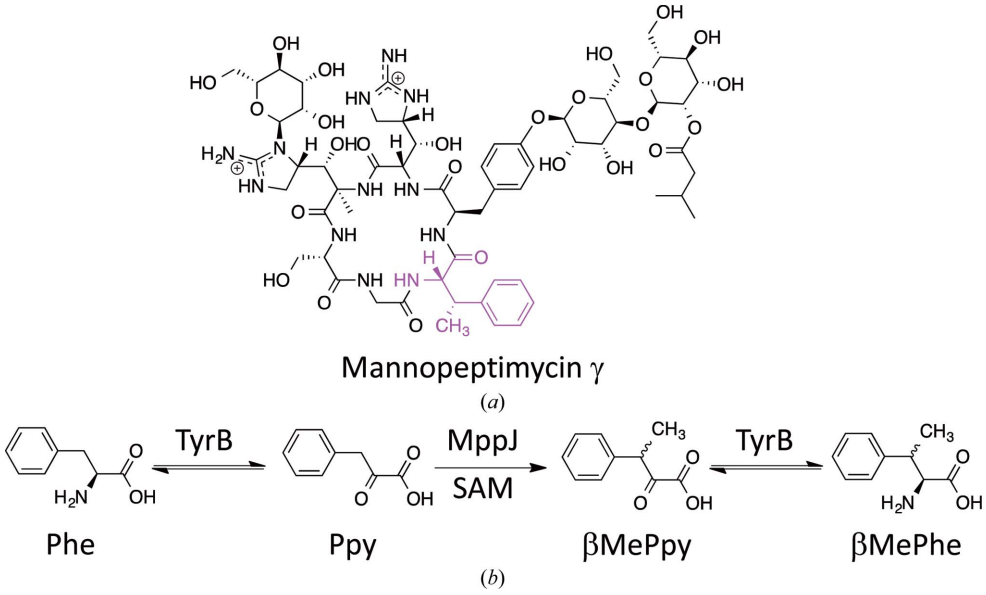

Figure 1
Chemical structure and biosynthesis of β-methylphenylalanine. (*a*) Mannopeptimycin. (*b*) MppJ catalyzes the formation of β-MePpy at the expense of one molecule of SAM. TyrB is an aromatic amino acid-specific transaminase.

gene in the cluster was elucidated to code for the MT that methylates the benzylic C atom of phenylpyruvate (Ppy) instead of phenylalanine (Phe) or the mannopeptimycin aglycone (Fig. 1*b*; Huang *et al.*, 2009; Magarvey *et al.*, 2006). The benzylic C atom of Ppy is slightly acidic, but its ability to act as an operational nucleophile remains to be established. When the methyl acceptor is carbon (CMT) rather than oxygen (OMT) or nitrogen (NMT), the reaction mechanisms become more complicated and are highly dependent on the electronic properties of the acceptor molecules (Lin, 2011). The purified MT displays a turquoise color (Supplementary Fig. S1[1]), implying the involvement of a metal ion(s), which is at odds with the known Ca^{2+}/Mg^{2+}-dependent OMTs (which are colourless; Akey *et al.*, 2011; Gómez García *et al.*, 2010; Kopycki *et al.*, 2008) and radical SAM-dependent enzymes (Duschene *et al.*, 2009; Frey *et al.*, 2008). Understanding this property may shed light on how MppJ executes the stereospecific *C*-methylation.

Natural products usually can be decoded into structurally unique subunits, such as nonproteinogenic/proteinogenic amino acids, deoxy/amino/acidic sugars, homo/heteroatom rings, polyketones *etc.*, where methylation often occurs (Thibodeaux *et al.*, 2007, 2008). Methylation can improve the physicochemical and pharmacological properties of natural products (Struck *et al.*, 2012; Zubieta *et al.*, 2001). Methylation is also part of the protection chemistry preventing sensitive functional groups from unwanted modifications and thus controlling the reaction fidelity towards the correct end products (Zubieta *et al.*, 2001). Understanding of the catalytic mechanism could facilitate efforts to engineer and transform existing natural products into new analogues with the desired medicinal efficacy (Liu *et al.*, 2011; Chan *et al.*, 2011). Here, we present the first crystal structures of a ferric ion SAM-dependent MT that illustrate four binary and ternary complexes in multiple reaction phases. This discovery further prompted us to convert MppJ into a structurally and functionally unrelated enzyme. Six stepwise engineering steps were validated by crystal structures. In combination with manipulation of coordination chemistry, we were able to engineer MppJ to perform both nonhaem-dependent hydration and OMT reactions for the first time.

2. Materials and methods

2.1. Protein expression and purification

The *mppJ* gene was amplified from *Streptomyces hygroscopicus* NRRL3085 genomic DNA by PCR. The product was ligated according to the manufacturers' instructions (Novagen) into the pET-28a(+) expression vector, which affords N-terminally His_6-tagged protein. A single colony was grown overnight in LB medium with kanamycin at 37°C. The overnight culture was inoculated with 50 times the volume of pre-warmed LB medium and grown at 37°C until the OD_{600} reached 0.6. 1 ml isopropyl β-D-1-thiogalactopyranoside (IPTG) was used to induce protein expression. Protein expression was induced at 16°C with shaking at 200 rev min^{-1} for 16 h. Cell pellets were collected and suspended in lysis buffer consisting of 20 m*M* Tris–HCl pH 8.0, 500 m*M* NaCl, 10% glycerol, 10 m*M* imidazole, 0.5 m*M* phenylmethanesulfonyl fluoride (PMSF). A sonicator or a microfluidizer was used to lyse the cells. The His_6-tagged target protein could be extracted from the lysate by batch Ni^{2+}–NTA agarose (Qiagen). The lysate–Ni^{2+}–NTA agarose mixtures were loaded into a column equilibrated with lysis buffer. Wash buffer consisting of 20 m*M* Tris–HCl pH 8.0, 500 m*M* NaCl, 10% glycerol, 40 m*M* imidazole was used to remove back-

[1] Supporting information has been deposited in the IUCr electronic archive (Reference: DW5091).

ground proteins, and the same buffer with 250 m*M* imidazole was used to elute the desired proteins. The purity was checked by denaturing SDS–PAGE and visualized by Coomassie Brilliant Blue staining. The purified proteins were concentrated by ultrafiltration and the buffer was exchanged to remove excess imidazole and ions by several iterations of the dilution/reconcentration procedure. The final protein at the desired concentration that contained glycerol at up to 50% was stored at −20°C. Gel-filtration analysis was performed using an ÄKTA FPLC system equipped with a HiLoad Superdex 200 column (Amersham Bioscience) under an isocratic condition (50 m*M* HEPES pH 8.0). Protein concentrations were estimated using the Bradford assay.

2.2. Crystallization and data collection

The purified protein in buffer solution (50 m*M* HEPES pH 7.5, 100 m*M* $CaCl_2$) was concentrated to 24 mg ml^{-1} and 6 m*M* SAM and Ppy were added for crystallization. The initial crystallization condition was determined with a sparse crystallization matrix at 20°C using the hanging-drop vapour-diffusion technique. The optimized crystallization condition consisted of 16% PEG 3350, 200 m*M* NaI and the drops were comprised of 1 ml protein solution and 1 ml reservoir solution. Crystals were obtained within 10 d. Crystals were transferred into the crystallization buffer with an additional 20% ethylene glycol and flash-cooled in liquid nitrogen before data collection. X-ray diffraction data sets were collected on ADSC Quantum 315 or Quantum 210 CCD detectors on beamlines 13B1 and 13C1 of the National Synchrotron Radiation Research Center (Taiwan) and beamlines 12B2 and 44XU of Spring-8 (Japan) and using in-house X-ray crystallography facilities. Data were indexed and scaled with the *HKL*-2000 package (Otwinowski & Minor, 1997). The contents of the asymmetric units were estimated from the Matthews coefficient (Kantardjieff & Rupp, 2003). The data suggest a value of 2.29 Å^3 Da^{-1} with 46.3% solvent content, corresponding to two molecules per asymmetric unit in the crystal.

2.3. Structure determination and refinement

The multiple-wavelength anomalous dispersion (MAD) method was used to obtain phase information, and *CRANK* (Ness *et al.*, 2004) was used to find the phase solution. The *CRANK* pipeline started with substructure detection and ended with model building, and included procedures for substructure detection by *AFRO*/*CRUNCH*2 (De Graaff *et al.*, 2001), substructure refinement by *BP*3 (Pannu & Read, 2004), hand determination and density modification by *SOLOMON* (Abrahams & Leslie, 1996) and model building by *Buccaneer* (Cowtan, 2006, 2008). Phase extension yielded electron-density maps into which a polypeptide model was built with *Coot* (Emsley & Cowtan, 2004; Emsley *et al.*, 2010). The model was further refined with *REFMAC* (Murshudov *et al.*, 2011). Other native structures were solved by the molecular-replacement method using SeMet-substituted MppJ as the search model. Figures were generated using *PyMOL* (http://www.pymol.org). Detailed refinement statistics are given in Table 1.

3. Results and discussion

3.1. Protein crystallization and structure determination

Recombinant MppJ, encoding 337 amino acids (38 kDa), was expressed in *Escherichia coli* as an N-terminally His_6-tagged protein and was purified sequentially by Ni^{2+}-affinity chromatography/ion-exchange chromatography (an option for metal-ion determination) and gel-filtration chromatography (Supplementary Fig. S2). MppJ was cocrystallized in the presence of SAM and Ppy. Although MppJ is structurally related to the MT protein family (Supplementary Fig. S3), the phase problem could not be solved using molecular replacement (MR). Selenomethionine-labelled protein was then pursued, the crystals of which diffracted to 2.0 Å resolution. The Se peak wavelength was used to obtain the initial phase by multiple-wavelength anomalous dispersion (MAD). The Se anomalous peaks were used to build the initial model (*CRANK*; Ness *et al.*, 2004). The final model displays correct stereochemistry, with 99.5% of residues in the allowed region of the Ramachandran plot. Data-collection and refinement statistics are summarized in Table 1. From the collected crystal diffraction data, we obtained an additional four structures of MppJ in complex with Ppy, 4-hydroxyphenylpyruvate (4HPpy), SAM and Ppy or SAH and MePpy, although crystals of the apo form remained unobtainable.

3.2. Overview of the structure

MppJ is a homodimer based on gel filtration and analytical ultracentrifugation (determined molecular mass of 70.2 kDa; calculated molecular mass for a dimer of 74.4 kDa; Fig. 2*a*). Consistently, each asymmetric unit contains two densely packed MppJ molecules (Supplementary Fig. S4). Most SAM-dependent MT structures share a core Rossmann nucleotide-binding fold (α/β-sandwich fold; Schubert *et al.*, 2003; Martin & McMillan, 2002). This core is elaborated with additional structural elements evolved for highly variable functions, according to which MTs have been grouped into five classes (classes I–V; Schubert *et al.*, 2003; Martin & McMillan, 2002). MppJ belongs to the class I fold, in which a single polypeptide consists of two domains (Fig. 2*b*; Supplementary Fig. S5): an extended N-terminal dimerization domain (DD domain; residues 1–160) and a C-terminal methyltransfer core domain (MT domain; residues 161–337). The DD domain features an antiparallel three-stranded β-sheet core (β1–β3) confined by two helices (α1 and a fractured long helix α5–α8) in a forceps-like arrangement. These two helices extend from one DD domain, protruding into the DD domain of the other subunit for protein dimerization (Supplementary Fig. S6). The DD domain also helps to shape a substrate-binding pocket at the occlusion of the DD and MT domains (Fig. 2*c*). The MT domain is composed of a seven-stranded β-sheet core (β4–β10) sandwiched by three α-helices on one side (α10–α12) and

Table 1
Data-collection, phasing and refinement statistics for structures of MppJ and mutants thereof.

Values in parentheses are for the highest resolution shell.

	SeMppJ–SAH–MePpy					
	Peak	Inflection	Remote	MppJ–SAM–Ppy	MppJ–Ppy	MppJ–4HPpy
Data collection						
Space group	$P2_12_12_1$			$P2_12_12_1$	$P2_12_12_1$	$P2_12_12_1$
Unit-cell parameters						
a (Å)	64.3			57.5	57.4	59.5
b (Å)	78.0			93.5	88.7	81.1
c (Å)	138.2			142.2	137.0	137.4
$\alpha = \beta = \gamma$ (°)	90.0			90.0	90.0	90.0
Wavelength	0.97874	0.97893	0.96353	1.54	0.90	0.97
Resolution (Å)	30.0–2.00 (2.07–2.00)	30.0–2.00 (2.07–2.00)	30.0–2.00 (2.07–2.00)	19.0–2.45 (2.54–2.45)	30.0–2.50 (2.59–2.50)	30.0–2.40 (2.49–2.40)
R_{sym} or R_{merge} (%)	11.0 (72.3)	10.5 (72.2)	11.0 (75.1)	8.5 (61.4)	12.2 (62.0)	13.7 (58.9)
$\langle I/\sigma(I)\rangle$	23.3 (3.25)	16.5 (2.24)	16.3 (2.29)	15.7 (2.06)	13.3 (2.67)	12.5 (2.94)
Completeness (%)	99.9 (100.0)	99.9 (99.8)	99.9 (99.8)	97.1 (90.4)	99.1 (98.6)	93.5 (96.0)
Multiplicity	10.3 (10.2)	5.2 (5.1)	5.1 (5.1)	4.2 (3.9)	4.9 (5.0)	5.0 (5.1)
Refinement						
Resolution (Å)	2.00			2.45	2.50	2.40
No. of reflections	45227			27511	23457	23694
R_{work}/R_{free}	0.201/0.256			0.171/0.238	0.174/0.248	0.172/0.248
No. of atoms						
Protein	5200			5186	5246	5170
Ligand/ion	102/7			102/16	60/6	52/11
Water	625			299	347	358
B factors (Å^2)						
Protein	29.2			42.9	36.6	33.0
Ligand/ion	27.7/34.0			37.3/44.8	36.6/43.4	31.3/42.7
Water	39.1			39.3	33.7	33.8
R.m.s deviations						
Bond lengths (Å)	0.009			0.013	0.012	0.012
Bond angles (°)	1.400			1.649	1.569	1.542

	MppJ D244E	MppJ D244L	MppJ R127L/D244E	MppJ R127L/V300E	MppJ R127L/D244A/V300E	MppJ (SAH/Ppy) R127L/D244A/V300E
Data collection						
Space group	$P2_12_12_1$	$P2_12_12_1$	$P2_12_12_1$	$P2_12_12_1$	$P2_12_12_1$	$P2_12_12_1$
Unit-cell parameters						
a (Å)	57.0	57.2	60.8	60.9	61.0	57.4
b (Å)	90.2	89.6	93.7	97.1	96.8	89.9
c (Å)	136.5	136.6	137.4	135.2	135.4	137.6
$\alpha = \beta = \gamma$ (°)	90.0	90.0	90.0	90.0	90.0	90.0
Wavelength	0.97	0.90	1.00	1.00	1.00	1.00
Resolution (Å)	30.0–2.30 (2.38–2.30)	30.0–2.50 (2.59–2.50)	30.0–2.20 (2.28–2.20)	30.0–2.10 (2.18–2.10)	30.0–2.00 (2.07–2.00)	30.0–2.20 (2.24–2.20)
R_{sym} or R_{merge} (%)	9.9 (59.5)	9.5 (66.9)	6.9 (54.6)	8.7 (52.1)	5.7 (47.2)	7.6 (64.4)
$\langle I/\sigma(I)\rangle$	16.6 (3.0)	19.1 (3.2)	25.0 (3.3)	19.4 (3.7)	26.6 (3.5)	22.6 (2.8)
Completeness (%)	100.0 (100.0)	99.9 (100.0)	99.9 (100.0)	99.9 (100.0)	99.9 (100.0)	99.9 (100.0)
Multiplicity	4.9 (4.9)	6.1 (6.2)	6.1 (6.2)	6.2 (6.2)	5.8 (5.3)	6.0 (6.1)
Refinement						
Resolution (Å)	2.30	2.50	2.20	2.10	2.00	2.20
No. of reflections	30264	24097	34611	43121	48442	31111
R_{work}/R_{free}	0.165/0.227	0.182/0.255	0.162/0.229	0.147/0.196	0.155/0.211	0.169/0.234
No. of atoms						
Protein	5232	5246	5173	5182	5169	5224
Ligand/ion	102/7	102/6	102/17	104/10	104/16	102/6
Water	427	331	529	759	788	496
B factors (Å^2)						
Protein	34.9	52.4	31.2	26.3	29.4	35.8
Ligand/ion	43.6/58.8	56.1/70.7	32.8/42.8	36.6/37.9	34.0/40.3	40.9/36.4
Water	40.5	47.5	35.8	39.6	41.8	39.4
R.m.s deviations						
Bond lengths (Å)	0.010	0.009	0.016	0.019	0.020	0.015
Bond angles (°)	1.415	1.380	1.775	1.946	2.032	1.713

another three on the other side (α13, α14 and α16) (Fig. 2*b*). All of the strands except for β10 run in parallel. A short 3_{10}-helical segment (η3) situated between β7 and α14 is highly conserved in a typical MT fold. Two additional 3_{10}-helical segments (η1 and η2) are unique and are not found in other MT folds.

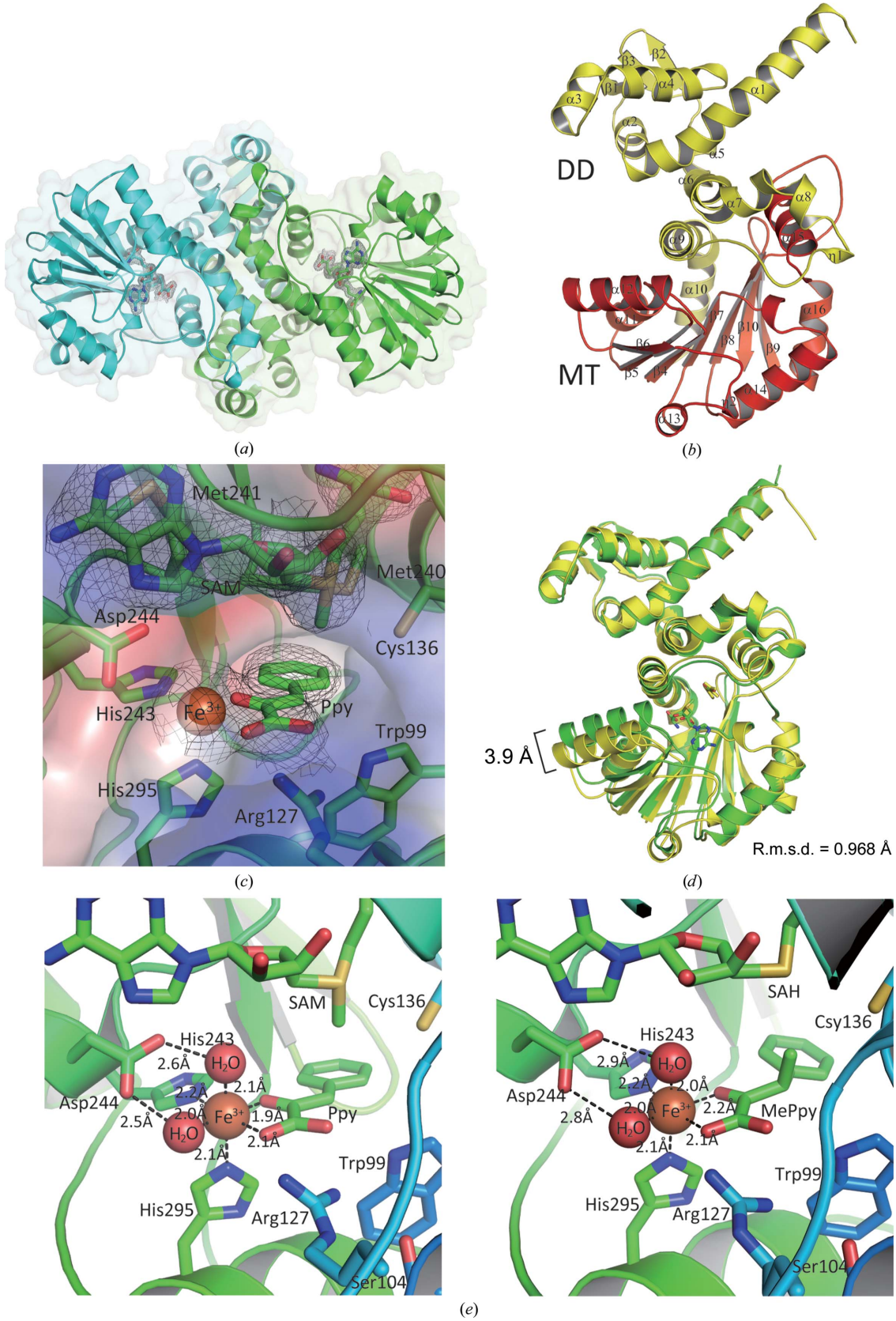

Figure 2
Structures of MppJ. (*a*) An asymmetric unit contains two MppJ polypeptides. (*b*) MppJ is composed of two domains: a dimerization domain (DD) and a methyltransfer domain (MT). (*c*) The substrate-binding pocket is situated at the occlusion of the DD and MT domains, in which the iron centre is solvent-accessible. (*d*) Superposition of binary (Ppy) and ternary (Ppy and SAM) structures revealed a protein conformational change (r.m.s.d. of 0.968 Å for 334 C^{α} atoms of MppJ); the binary and ternary structures are coloured yellow and green, respectively. (*e*) Structures of the MppJ–SAM–Ppy (left) and MppJ–SAH–MePpy (right) complexes.

3.3. Conformational change and SAM/SAH binding

Superposition of binary (Ppy) and ternary (Ppy and SAM) structures (r.m.s.d. of 0.968 Å for 334 C^{α} atoms of MppJ) revealed that the MT domain undergoes a modest conformational change when SAM is bound (Fig. 2*d*). Upon binding of SAM, β5, β6 and α12 together move towards α9, resulting in an overall displacement of 3.9 Å. Two conserved motifs are commonly found in a typical MT fold: a glycine-rich sequence (motif I) that interacts with the methionine portion of SAM, and an acidic loop (motif II) that interacts with the ribose moiety (Schubert *et al.*, 2003; Martin & McMillan, 2002). The former (D*X*G*X*G*X*G) is located between β4 and α11, while the latter is placed between β5 and α12. Asp164 may interact with the amino group of methionine (see Supplementary Fig. S3 for a sequence alignment with representative homologues; Schubert *et al.*, 2003; Martin & McMillan, 2002). In ternary structures the electron density of SAM/SAH is well defined across the top of the MT fold (Fig. 2*c*). The ribose lies above the carboxyl end of β4, where the C2 and C3 hydroxyl groups interact with the backbone N atoms of Gly168 and Ala191. The methionine moiety stretches out between α9 and α11, where the carboxylate group forms a salt bridge with the guanidino group of Arg172 and the amino group interacts with the backbone O atoms of Gly166 and Phe239. The adenine ring is confronted with residues between β6 and η2.

3.4. Ppy binding site and coordination chemistry

A chunk of electron density adjacent to SAM/SAH was observed in the ternary structures which is fitted well by Ppy/MePpy (Fig. 2*c* for the SAM–Ppy form). The phenyl portion of Ppy/MePpy is surrounded by hydrophobic and van der Waals residues (Fig. 2*c*). A round bulk of additional electron density offside the α-ketoacid of Ppy/MePpy was also observed, which is likely to be a mononuclear metal ion (Fig. 2*c*). Using inductively coupled plasma mass spectrometry (ICP-MS), synchrotron rapid-scanning X-ray fluorescence (SRS-XRF) and X-ray absorption spectroscopy (XAS) analysis, the metal ion was determined to be a ferric ion (Supplementary Fig. S7), the first case in the MT enzyme family. The metal is essential for the MT reaction and protein stabilization, as no product was detected in enzymatic reactions with added EDTA and the protein is prone to precipitation (5 m*M*; data not shown). In addition to the bidentate Ppy/MePpy, the mononuclear ferric ion coordinates to residues His243, Asp244 and His295, where His243 and Asp244 are positioned on the η3 immediate C-terminus of β7 and His295 is situated at the C-terminus of α15 (Fig. 2*e*). This 2-His-1-carboxylate facial triad confines the active-site metal ion: the $N^{\varepsilon 2}$ atom of His243 (2.2 Å), the α-ketoacid bidentate of Ppy/MePpy and water A (2.0 Å) form the equatorial plane and water B (2.0 Å) and the $N^{\varepsilon 2}$ atom of His295 (2.1 Å) occupy apical positions (Fig. 2*e*), which are common to all nonhaem iron(II) oxygenases (Dunwell *et al.*, 2004; Dunwell, 1998). These oxygenases share a common jelly-roll fold (a cupin fold; Dunwell *et al.*, 2004; Dunwell, 1998) and can be categorized into three groups based on the spacing of the three residues in the primary structure. In terms of primary structure, the HDX_{51}H motif of MppJ may be assigned to the HX(D/E)$X_{50\text{–}210}$H group, the most general spacing motif for nonhaem iron(II) oxygenases (Conrad & Moran, 2008; Brownlee *et al.*, 2008; Purpero & Moran, 2007; Moran, 2005; Dunwell *et al.*, 2004). Ppy/MePpy contacts the active-site metal ion through an asymmetric bidentate coordination, one carboxylate O atom (2.1 Å) and the adjacent α-oxylate/keto O atom (1.9/2.2 Å), forming a tetragonal bipyramidal structure in which the benzylic C atom of Ppy/MePpy adopts an enol/keto configuration and the carboxylic group of Ppy/MePpy interacts electrostatically with the guanidino group of Arg127 (3.0 Å) (Fig. 2*e*). In analogy to nonhaem iron(II) α-ketoacid-dependent oxygenases, the coordination of Ppy to iron(III) leads to the formation of thermodynamically stable high-spin ferric Ppy complexes with rhombic octahedral symmetry (S = 5/2, isotropic $g \simeq 4.3$; Fig. 3*a*). In contrast, two water molecules sandwiched by the ferric ion and the carboxylic group of Asp244 together form a hexacoordinate species, compared with the pentacoordination in the nonhaem iron(II) α-ketoacid-dependent oxygenases. The two water molecules in the methyltransfer reaction may prevent the nonhaem iron(II) α-ketoacid-dependent oxygenase-like reactions from occurring (see below), whereupon the formation of hydroxyl products, H_2O_2 and radicals (radical-scavenging assay) as leaky byproducts was not detected (data not shown).

3.5. Reaction mechanism

MT-catalyzed reactions proceed in most cases by direct transfer of the methyl group from SAM to acceptors *via* an S_N2-like mechanism. This process usually requires activation of the OH/NH_2 nucleophile through deprotonation. In OMTs, *e.g.* chalcone OMT, isoflavine OMT (Zubieta *et al.*, 2001) and RebM (Zhang *et al.*, 2008; Singh *et al.*, 2008), a His residue is recruited to deprotonate the targeted hydroxyl group in the acceptors. In metal-dependent OMTs, metal ions may play dual roles in substrate binding and hydroxyl polarization. MycE supports a mechanism in which a conserved His acts as a general base and an Mg^{2+} ion positions the methyl acceptor as well as stabilizing the resulting hydroxylate. Rat catechol OMT (rOMT; Vidgren *et al.*, 1994) and plant flavonoid OMT (PFOMT; Männistö & Kaakkola, 1999) share a common structural motif where the methyl transfer proceeds with one hydroxyl group ionized by Mg^{2+} and a conserved Lys facilitates the methyl transfer (Schluckebier *et al.*, 1995). NovP catalyzes the penultimate step in the biosynthesis of the aminocoumarin antibiotic novobiocin. Along with a possible metal ion, a conserved Asp residue is likely to act as the general base deprotonating the 4-OH group of the noviose unit.

In MppJ the benzylic C atom of Ppy is perfectly situated between the methyl group of SAM (3.3 Å) and residue Trp99 (3.6 Å) (Fig. 2*e*, left). On the basis of the detailed active-site structure, we propose the mechanism shown in Fig. 4(*a*). In this mechanism, the ferric ion serves as a Lewis acid catalyst facilitating the formation of a Ppy enolate. On the collapse of the α-enolate the resulting benzylic carbanion can then attack

the methylium of SAM to form βMePpy (keto form) *via* S_N2 nucleophilic substitution. Our structural results have provided support for this mechanism, as shown by the Ppy and βMePpy complexed structures, in which the sulfur leaving group, methylium electrophile and benzylic carbon nucleophile are aligned in a straight line, providing the best overlap between the lone pair of the nucleophile and the C—S σ^* antibonding orbital for concerted bond breakage/formation (Figs. 4*b* and 4*c*). However, detailed testing of the mechanism will require in-depth investigations in the future, including dissection of microscopic steps and determination of rate-limiting steps. Here, we report the specific activities of site-specific mutants of key residues at the active site. As shown by the data in Supplementary Table S1, the mutants that are likely to perturb the binding of the ferric ion also lead to significant loss in activity, while only modest basicity was observed for the W99F and S104A mutants. Based on these results, we hypothesize that the ferric ion plays key roles in the catalysis of MppJ, including substrate binding, Lewis acid polarization, transition-state stabilization and reaction-path alignment. This identifi-

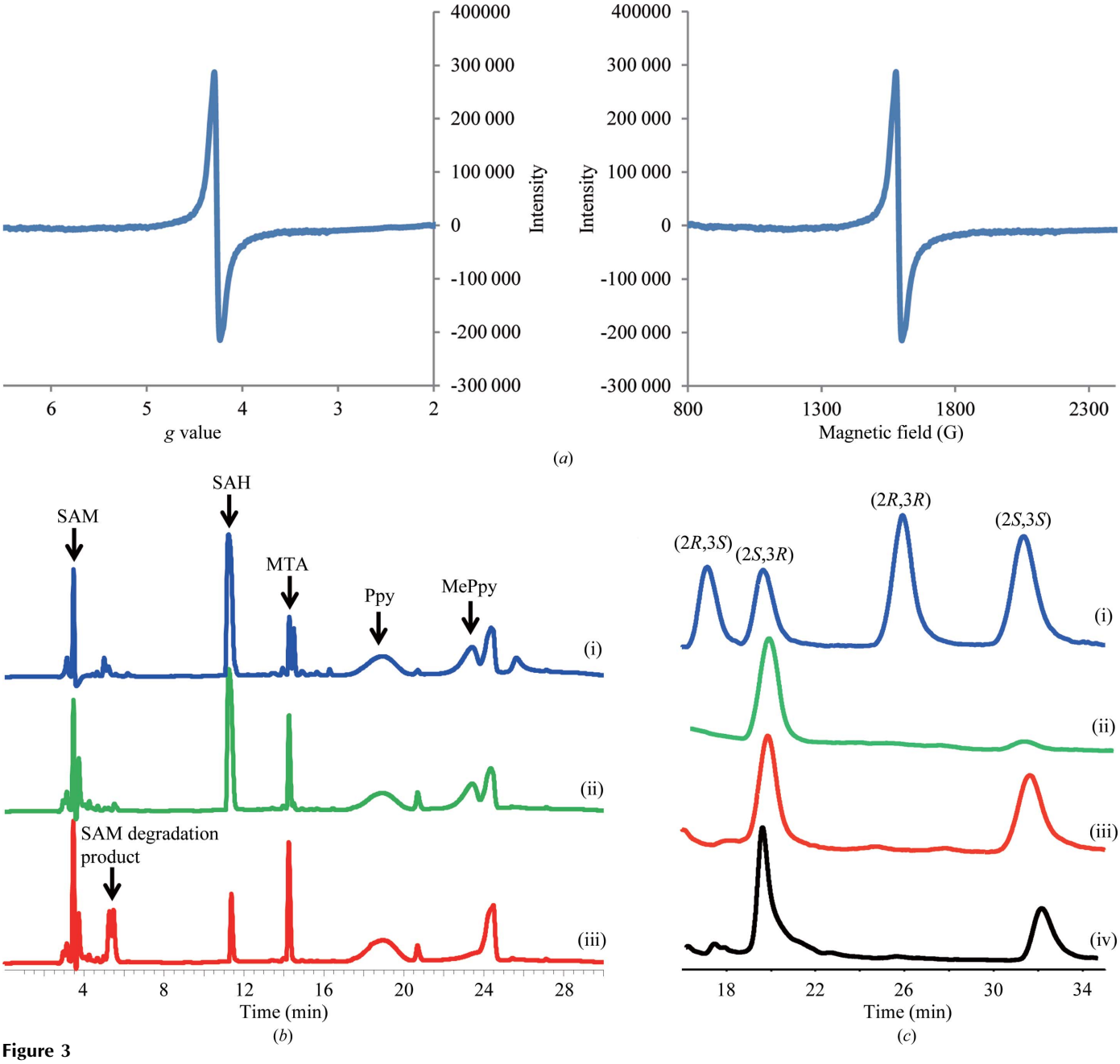

Figure 3
EPR spectra and HPLC traces. (*a*) EPR analyses of MppJ. The metal is determined to be a high-spin ferric ion (S = 5/2, $g \simeq 4.3$). (*b*) LC traces of enzymatic reactions for MppJ: (i) WT, (ii) D244E and (iii) D244L. Ppy, phenylpyruvate; MePpy, β-methylphenylpyruvate; SAM, *S*-adenosylmethionine; SAH, *S*-adenosylhomocysteine; MTA, 5′-methylthioadenosine (a degradation product). (*c*) (i) Four enantiomers of β-methylphenylalanine (βMePhe) resolved by chiral HPLC. (ii) Enzymatic products of MppJ and TyrB (an aromatic amino acid-specific transaminase) at 4 h. (iii) Enzymatic products of MppJ and TyrB at 8 h. (iv) Enzymatic products of MppJ W99F and TyrB at 8 h.

cation specifies the rationale with respect to how MppJ takes advantage of iron-coordination chemistry to alter the electronic properties of the acceptor molecule for stereospecific *C*-methylation.

On the other hand, the turquoise colour may be related to the iron–sulfur interaction (Kovacs & Brines, 2007; Lugo-Mas *et al.*, 2006). The nearby residues Met240 and Met241 were mutated to leucine, which negated their roles in colour formation. The enzyme activities of the M240L, M241L and double mutants decreased moderately (Supplementary Table S1), suggesting roles in SAM binding instead of coordination chemistry. Ppy and SAM have a similar binding affinity to MppJ (K_d = 14.6 and 22.4 µ*M*, respectively; Supplementary Fig. S8); however, that of SAH is one order of magnitude (K_d = 2.5 µ*M*) greater than that of Ppy/SAM. Taken together, Ppy may bind to MppJ first; SAM then enters and elicits a conformational change to better align the methyl-transfer path. Once the reaction has completed, MePpy dissociates prior to SAH. MppJ then re-adopts the initial state for the next cycle of the MT reaction.

3.6. MppJ is an *R*-configuration-specific MT

(2*S*,3*S*)-*β*-Methylphenylalanine (*β*MePhe) is the third residue in mannopeptimycin (Fig. 1*a*; He *et al.*, 2002). The ligand turned out to be (3*R*)-*β*MePpy in the solved structure (Fig. 4*c*) as opposed to the expected *S* configuration (Huang *et al.*, 2009). We hence re-determined the chirality of the MT product *β*MePpy. Reactions with added MppJ and the

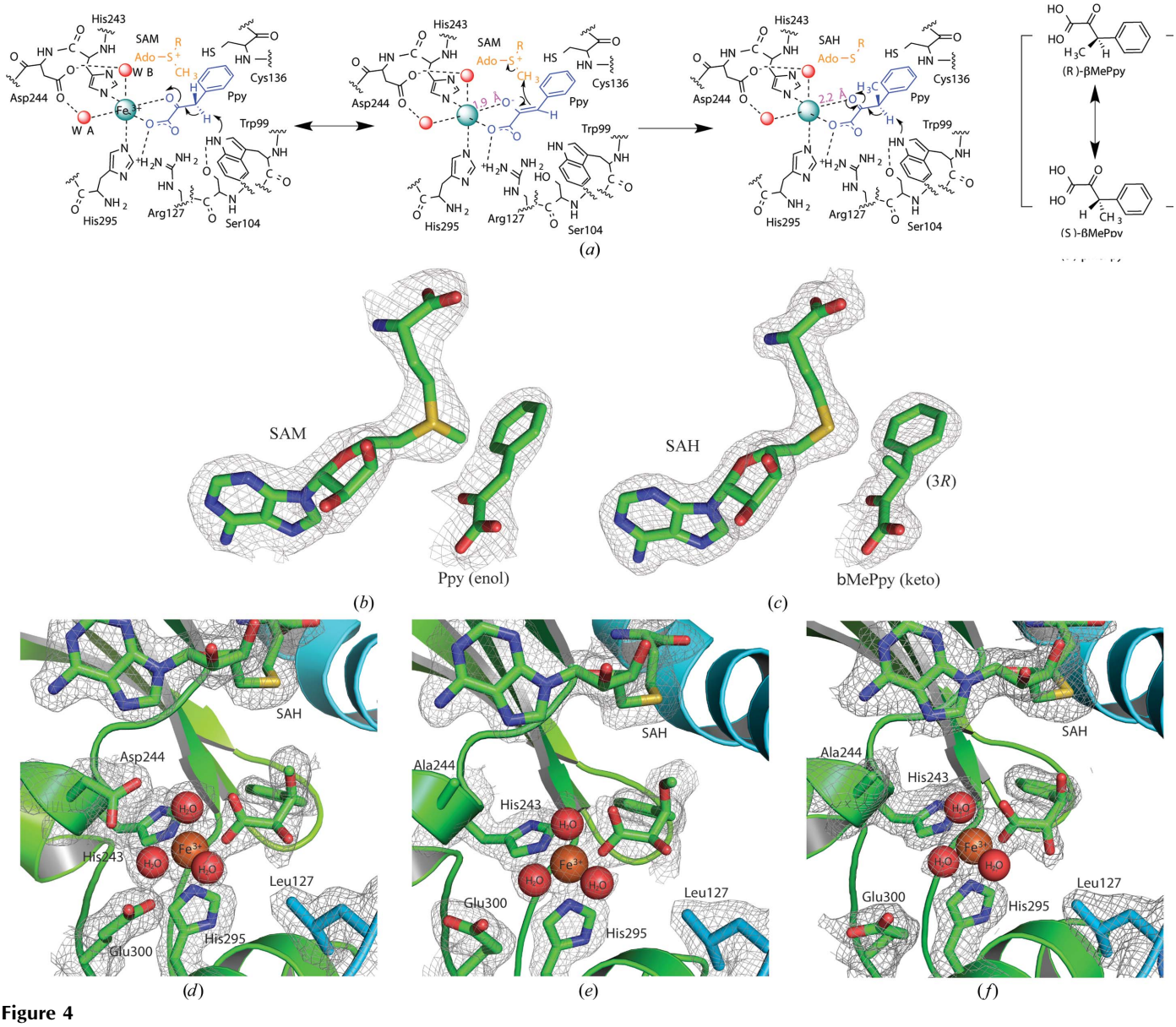

Figure 4
Active sites and proposed mechanism for MppJ and mutants thereof. (*a*) The proposed methyltranferation mechanism of MppJ. (*b*, *c*) Structures of SAM–Ppy and SAH–MePpy in the MppJ complexes. The $2F_o - F_c$ electron-density maps are contoured at 1σ. (*d*) Active-site arrangement of the MppJ R127L/V300E double mutant. (*e*) Active-site arrangement of the MppJ R127L/D244A/V300E triple mutant in the presence of SAM and Ppy. (*f*) Active-site arrangement of the MppJ R127L/D244A/V300E triple mutant in the presence of SAH and Ppy.

(2*S*)-aromatic amino acid-specific transaminase TyrB were conducted, in which the resulting *β*MePpy was converted to *β*MePhe and resolved by chiral HPLC. LC traces showed ratios of 5:1 and 1:1 for (2*S*,3*R*)-*β*MePhe *versus* (2*S*,3*S*)-*β*MePhe in reaction courses of 4 and 8 h, respectively. The trace instead showed a ratio of 5:3 at 8 h when MppJ was substituted by the W99F mutant (Fig. 3*c*). The slower racemization suggests that Trp99 is involved in the conversion to some extent. Apparently, (3*R*)-*β*MePpy was first formed, which could undergo racemization by the enzyme or in solution owing to the relative acidity of the benzylic C atom (Fig. 4*a*). MppJ was thereby redefined as an *R*-configuration-specific MT. It is noteworthy that racemic (3*R*/*S*)-*β*MePpy can be converted to (2*S*,3*R*)/(2*S*,3*S*)-*β*MePhe by the aromatic amino acid-specific transaminase TyrB (Fig. 1*b*). Given that the transamination is reversible, both (2*S*,3*R*)- and (2*S*,3*S*)-*β*MePhe would re-establish a constant equilibrium when the latter is taken up upon incorporation into mannopeptimycin.

3.7. Post-translational modification (PTM)

Unexpectedly, an extra electron density placed in the cleft between *α*16 and *β*9 was identified in all of the structures solved (Figs. 5*c* and 5*d*). The density is best fitted with Ppy, while it is covalently linked to Cys319. The adduct was determined to be the diastereomer (2*S*,3*R*)-*β*-thioether-*α*-hydroxyphenylpropionic acid, which is likely to be formed by conjugated addition as result of the thiolate of Cys319 attacking the *β*-carbon of enolic Ppy from the *Re* face (refer to Supplementary Fig. S11 for mass-spectrometric analysis). The Ppy adduct is 22.3 Å away from the active site (3*R*)-*β*MePpy (Fig. 5*c*, Supplementary Fig. S10). Whether this remote modification influences the MT activity was examined. Cys319 was mutated to alanine and subjected to activity examinations and protein crystallization. C319A could not be crystallized, suggesting that the residue may have a structural role. Additionally, the MT activity declined moderately (61% relative to the wild type), suggesting that the residue or modification is involved to some extent in reaction regulation. To determine the timing of the post-translational modification (in cells or in test tubes), MppJ in complex with 4-hydroxyphenylpyruvate (4HPpy) was crystallized. The structure clearly showed that 4HPpy appears at both sites (Figs. 5*e* and 5*f*), one chelating with the iron centre and the other covalently linked to Cys319. Apparently, PTM took place in the test tube, suggesting that the modification is substrate-dependent and the MT activity is positively regulated.

3.8. MppJ has no nonhaem oxygenase activity

In nonhaem *α*-ketoacid-dependent oxygenases, the 2-His-1-carboxylate facial triad motif provides a scaffold to bind the

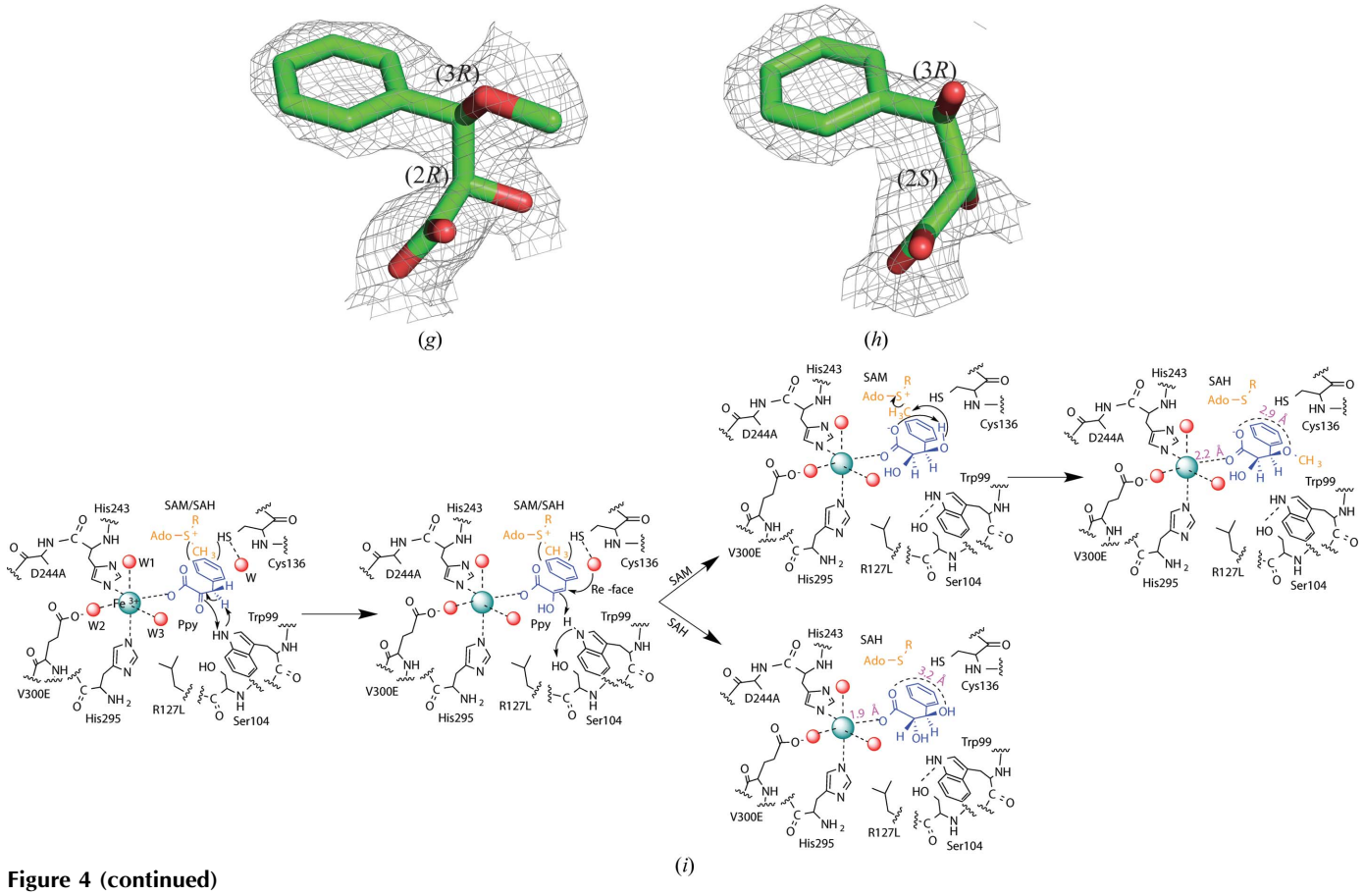

Figure 4 (continued)
(*g*) Structure and $2F_o - F_c$ electron-density map of (2*R*,3*R*)-*α*-hydroxy-*β*-methoxyphenylpropionic acid contoured at 1*σ*. (*h*) Structure and $2F_o - F_c$ electron-density map of (2*S*,3*R*)-*α*,*β*-dihydroxy-phenylpropionic acid. (*i*) The proposed hydration–methylation mechanism.

iron(II) centre, while retaining the flexibility to bind additional exogenous electron-rich ligands (*e.g.* α-ketoacids) to the iron(II) coordination sphere (forming a pentacoordinate species) necessary for activation of molecular oxygen (as the sixth coordinate) at the iron(II) centre (Costas *et al.*, 2004; Solomon *et al.*, 2000). Given that MppJ possesses traits of a typical nonhaem α-ketoacid-dependent oxygenase but lacks intrinsic dioxygenase activity, we hypothesized that the

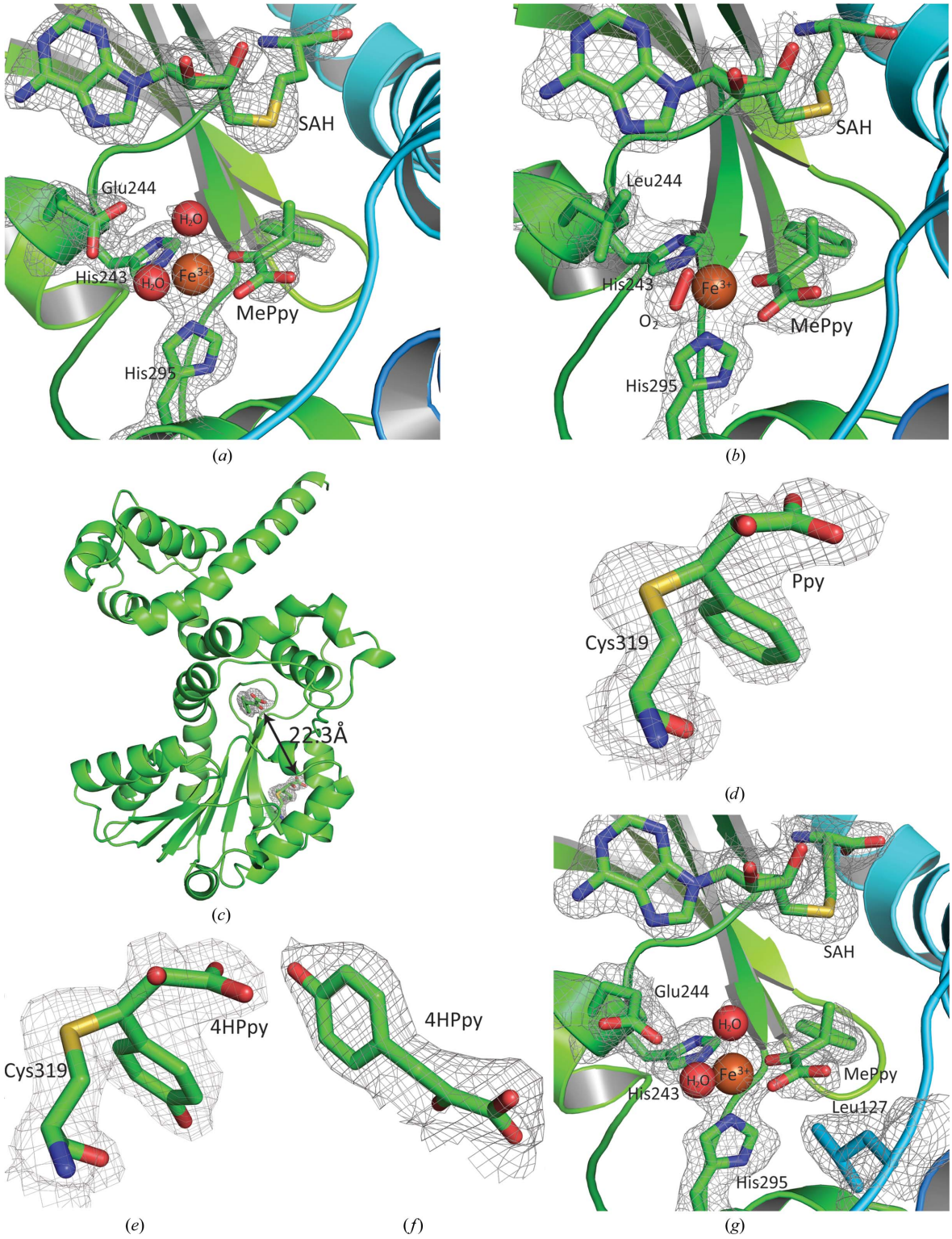

Figure 5
Structures of MppJ mutants and post-translational modification. (*a*) Active-site arrangement of the MppJ D244E mutant. (*b*) Active-site arrangement of the MppJ D244L mutant, where dioxygen is side-on the iron centre. (*c*) Ppy is covalently linked to Cys319, which is 22.3 Å away from the reaction centre. (*d–f*) Structures of Ppy-Cys, 4HPpy-Cys and 4HPpy; the $2F_o - F_c$ electron-density map is contoured at 1σ. (*g*) Active-site arrangement of the MppJ R127L/D244E double mutant.

inactivity could be ascribed to saturation of coordination. Note that two water molecules are confined between the iron centre and Asp244, where the iron–water (2.1 Å) and water–carboxylate (2.5 and 2.6 Å) distances are in the 'short strong hydrogen bond' (SSHB) and near the 'low-barrier hydrogen bond' (LBHB) ranges, respectively (Fig. 2*e*; Decker & Solomon, 2005; Gerlt *et al.*, 1997). It is likely that the two water molecules are bound tightly, thus preventing O_2 from taking the sixth coordination position. To test this hypothesis, D244E and D244L mutants were examined for their influence on coordination. Interestingly, the original turquoise colour became deepened in the D244E mutant, but changed to olive green in the D244L mutant (Supplementary Fig. S1), suggesting that the sandwiched water is related to ligand coordination and charge transfer. Nonhaem oxygenase assays (the conversion of Ppy to mandelate/homogentisate) were performed, but no product was found for either mutant. On the other hand, the relative yield of βMePpy increased in the D244E assay, while the co-substrate SAM seemed to undergo fragmentation in the D244L assays [mixed degradation products and 5-methylthioadenosine (MTA); Fig. 3*b*]. We then solved the crystal structures of D244E and D244L in complex with SAM and Ppy in a bid to explain the above observations. In the D244E structure the water–carboxylate distance was apparently shortened to the 'low-barrier hydrogen bond' (LBHB) range (Fig. 5*a*) in correlation with the colour enhancement, and the α-keto acid remains bidentately chelated to the iron, while Ppy has been methylated in the structure. In the D244L structure the coordination chemistry is changed to pentacoordination, in which surprisingly dioxygen instead of water is side-on the iron centre (Fig. 5*b*). This is in line with the alteration in colour. We reasoned that fragmentation of SAM is likely to be the result of hydrogen abstraction by a peroxide species, as manifested in the density map, in which the bond between the S atom and 2-amino-butanoic acid is partially discontinuous (Supplementary Fig. S9).

3.9. Engineering MppJ to a nonhaem oxygenase and an *O*-methyltransferase

Since MppJ possesses traits of a nonhaem oxygenase, it was of interest to attempt to convert MppJ to the structurally/functionally unrelated hydroxymandelate synthase (HMS). Five mutants were constructed by permutation and combination of the facial triads in such a way as to obtain a proper coordination arrangement for this purpose. However, most of the mutants lost iron-binding ability and activity (Supplementary Table S1). Additionally, the residue Val300 in MppJ that may geometrically be closer to Glu in the 2-His-1-carboxylate facial triad of HMS was mutated to Glu (V300E). There was still no HMS activity for the double mutant D244A/V300E, while interestingly the methyltransfer activity of the single mutant V300E was enhanced (Supplementary Table S1). In a typical nonhaem dioxgenase the iron centre is commonly located at the hydrophobic centre of the β-barrel. We reasoned that in addition to the 'coordinative saturation' the lack of activity could also be ascribed to the iron centre, which is highly exposed to solvent (Fig. 2*c*), so that no sooner had oxo-iron(IV) formed than it was annihilated by the bulk solvent. Further engineering as described below led to the creation of mutants that were able to perform two unexpected chemical reactions: hydration and *O*-methylation.

As mentioned above, Arg127 is electrostatically associated with Ppy (Fig. 2*e*), an interaction that is not observed in HMS. We wondered whether this residue might exert this interaction to confine the enzyme reaction. The active-site coordination in the structure of R127L/D244E is slightly dissimilar to that of D244E, in which the two water molecules are no longer sandwiched by D244E while the α-keto acid of Ppy remains chelated to the iron centre (Fig. 5*g*). To alter the bidentate binding mode, we re-introduced V300E into the R127L mutants. Two mutants, R127L/V300E and R127L/D244A/V300E, were made and subjected to enzyme-activity examination. The results showed that while Ppy seemed to be consumed considerably, no major peaks were identified. To uncover this discrepancy, we then solved the structures of these two mutants (Figs. 4*d* and 4*e*). To our surprise, a new chemical was identified in both structures, which was determined to be (2*R*,3*R*)-α-hydroxy-β-methoxyphenylpropionic acid (Fig. 4*g*). In both structures the chemical adopts a new conformation with only the carboxyl group engaging in the coordination. We reasoned that Trp99 is likely to serve as a general base abstracting the pro-*S* proton from the benzylic C atom of Ppy to form an enol conformer. A water molecule assisted by Cys136 then adds to the benzylic C atom from the *Re*-face, and Trp99 reprotonates the α-carbon to form a hydrated adduct. The α,β-vicinal diol in the structure adopts the *gauche* configuration, making the carboxyl end within hydrogen-bonding distance (2.9 Å) of the β-OH. With the help of Cys136, the Lewis acid-polarized carboxylate anion then acts as the base to intramolecularly deprotonate the β-OH to attack the methylium group of SAM, forming the unusual (2*R*,3*R*)-diastereomer (Fig. 4*i*, upper path). To validate this proposed mechanism, we further crystallized the triple mutant with SAH in lieu of SAM. In this structure a new molecule identified in the equivalent space assumes a similar but not identical conformation to that in the structure with SAM. This molecule turned out to be (2*S*,3*R*)-α,β-dihydroxyphenylpropionic acid (Figs. 4*f* and 4*h*). The α,β-vicinal diol now takes the *anti* configuration with the carboxyl end slightly away from the β-OH (3.2 Å), suggesting that the water addition follows a thermodynamically favourable path in the presence of SAH (Fig. 4*i*, lower path). Importantly, the β-OH is now unmethylated, unambiguously confirming that the β-OH can undergo Lewis acid-assisted *O*-methylation in the presence of SAM.

4. Conclusions

In summary, having solved multiple complexed structures, we realised that for the stereospecific *C*-methyltransfer reaction MppJ has evolved to acquire a nonhaem iron centre able to bind and orient α-ketoacid substrates and has developed a

sandwiched bi-water device able to avoid the formation of the reactive oxo-iron(IV) species. Most remarkably, MT mutants were engineered for the first time to be able to perform both nonhaem iron-dependent hydration and *O*-methylation reactions through altering the coordination chemistry for stereospecific new compounds.

5. Related literature

The following are cited in the Supporting Information for this article: Krissinel & Henrick (2007), Ravel & Newville (2005) and Schuck (2000).

The research was supported by the National Science Council (NSC) of Taiwan (grants 98-2311-B-001-014-MY3 and 100-2311-B-001-018-MY3 to T-LL.) and Academia Sinica intramural funding. X-ray diffraction was carried out at the Protein Crystallography Facility at the National Synchrotron Radiation Research Center (NSRRC) supported by the National Research Program for Genomic Medicine and the NSC of Taiwan, ROC. We thank NSRRC, Taiwan and SPring-8 for beam time allocations.

References

Abrahams, J. P. & Leslie, A. G. W. (1996). *Acta Cryst.* D**52**, 30–42.
Akey, D. L., Li, S., Konwerski, J. R., Confer, L. A., Bernard, S. M., Anzai, Y., Kato, F., Sherman, D. H. & Smith, J. L. (2011). *J. Mol. Biol.* **413**, 438–450.
Brownlee, J., He, P., Moran, G. R. & Harrison, D. H. T. (2008). *Biochemistry*, **47**, 2002–2013.
Chan, H.-C., Huang, Y.-T., Lyu, S.-Y., Huang, C.-J., Li, Y.-S., Liu, Y.-C., Chou, C.-C., Tsai, M.-D. & Li, T.-L. (2011). *Mol. Biosyst.* **7**, 1224–1231.
Conrad, J. A. & Moran, G. R. (2008). *Inorg. Chim. Acta*, **361**, 1197–1201.
Costas, M., Mehn, M. P., Jensen, M. P. & Que, L. (2004). *Chem. Rev.* **104**, 939–986.
Cowtan, K. (2006). *Acta Cryst.* D**62**, 1002–1011.
Cowtan, K. (2008). *Acta Cryst.* D**64**, 83–89.
Decker, A. & Solomon, E. I. (2005). *Curr. Opin. Chem. Biol.* **9**, 152–163.
Dunwell, J. M. (1998). *Biotechnol. Genet. Eng. Rev.* **15**, 1–32.
Dunwell, J. M., Purvis, A. & Khuri, S. (2004). *Phytochemistry*, **65**, 7–17.
Duschene, K. S., Veneziano, S. E., Silver, S. C. & Broderick, J. B. (2009). *Curr. Opin. Chem. Biol.* **13**, 74–83.
Emsley, P. & Cowtan, K. (2004). *Acta Cryst.* D**60**, 2126–2132.
Emsley, P., Lohkamp, B., Scott, W. G. & Cowtan, K. (2010). *Acta Cryst.* D**66**, 486–501.
Fontecave, M., Atta, M. & Mulliez, E. (2004). *Trends Biochem. Sci.* **29**, 243–249.
Frey, P. A., Hegeman, A. D. & Ruzicka, F. J. (2008). *Crit. Rev. Biochem. Mol. Biol.* **43**, 63–88.
Gerlt, J. A., Kreevoy, M. M., Cleland, W. W. & Frey, P. A. (1997). *Chem. Biol.* **4**, 259–267.
Gómez García, I., Stevenson, C. E. M., Usón, I., Freel Meyers, C. L., Walsh, C. T. & Lawson, D. M. (2010). *J. Mol. Biol.* **395**, 390–407.
Graaff, R. A. G. de, Hilge, M., van der Plas, J. L. & Abrahams, J. P. (2001). *Acta Cryst.* D**57**, 1857–1862.
He, H., Williamson, R. T., Shen, B., Graziani, E. I., Yang, H. Y., Sakya, S. M., Petersen, P. J. & Carter, G. T. (2002). *J. Am. Chem. Soc.* **124**, 9729–9736.
Houge-Frydrych, C. S., Gilpin, M. L., Skett, P. W. & Tyler, J. W. (2000). *J. Antibiot.* **53**, 364–372.
Huang, Y.-T., Lyu, S.-Y., Chuang, P.-H., Hsu, N.-S., Li, Y.-S., Chan, H.-C., Huang, C.-J., Liu, Y.-C., Wu, C.-J., Yang, W.-B. & Li, T.-L. (2009). *Chembiochem*, **10**, 2480–2487.
Kantardjieff, K. A. & Rupp, B. (2003). *Protein Sci.* **12**, 1865–1871.
Kopycki, J. G., Rauh, D., Chumanevich, A. A., Neumann, P., Vogt, T. & Stubbs, M. T. (2008). *J. Mol. Biol.* **378**, 154–164.
Kovacs, J. A. & Brines, L. M. (2007). *Acc. Chem. Res.* **40**, 501–509.
Krissinel, E. & Henrick, K. (2007). *J. Mol. Biol.* **372**, 774–797.
Lin, H. (2011). *Bioorg. Chem.* **39**, 161–170.
Liu, Y.-C., Li, Y.-S., Lyu, S.-Y., Hsu, L.-J., Chen, Y.-H., Huang, Y.-T., Chan, H.-C., Huang, C.-J., Chen, G.-H., Chou, C.-C., Tsai, M.-D. & Li, T.-L. (2011). *Nature Chem. Biol.* **7**, 304–309.
Lugo-Mas, P., Dey, A., Xu, L., Davin, S. D., Benedict, J., Kaminsky, W., Hodgson, K. O., Hedman, B., Solomon, E. I. & Kovacs, J. A. (2006). *J. Am. Chem. Soc.* **128**, 11211–11221.
Magarvey, N. A., Haltli, B., He, M., Greenstein, M. & Hucul, J. A. (2006). *Antimicrob. Agents Chemother.* **50**, 2167–2177.
Männistö, P. T. & Kaakkola, S. (1999). *Pharmacol. Rev.* **51**, 593–628.
Martin, J. L. & McMillan, F. M. (2002). *Curr. Opin. Struct. Biol.* **12**, 783–793.
Moran, G. R. (2005). *Arch. Biochem. Biophys.* **433**, 117–128.
Murshudov, G. N., Skubák, P., Lebedev, A. A., Pannu, N. S., Steiner, R. A., Nicholls, R. A., Winn, M. D., Long, F. & Vagin, A. A. (2011). *Acta Cryst.* D**67**, 355–367.
Ness, S. R., de Graaff, R. A. G., Abrahams, J. P. & Pannu, N. S. (2004). *Structure*, **12**, 1753–1761.
Otwinowski, Z. & Minor, W. (1997). *Methods Enzymol.* **276**, 307–326.
Pannu, N. S. & Read, R. J. (2004). *Acta Cryst.* D**60**, 22–27.
Purpero, V. & Moran, G. R. (2007). *J. Biol. Inorg. Chem.* **12**, 587–601.
Ravel, B. & Newville, M. (2005). *J. Synchrotron Rad.* **12**, 537–541.
Schluckebier, G., O'Gara, M., Saenger, W. & Cheng, X. (1995). *J. Mol. Biol.* **247**, 16–20.
Schubert, H. L., Blumenthal, R. M. & Cheng, X. (2003). *Trends Biochem. Sci.* **28**, 329–335.
Schuck, P. (2000). *Biophys. J.* **78**, 1606–1619.
Singh, S., McCoy, J. G., Zhang, C., Bingman, C. A., Phillips, G. N. & Thorson, J. S. (2008). *J. Biol. Chem.* **283**, 22628–22636.
Solomon, E. I., Brunold, T. C., Davis, M. I., Kemsley, J. N., Lee, S.-K., Lehnert, N., Neese, F., Skulan, A. J., Yang, Y.-S. & Zhou, J. (2000). *Chem. Rev.* **100**, 235–350.
Struck, A. W., Thompson, M. L., Wong, L. S. & Micklefield, J. (2012). *Chembiochem*, **13**, 2642–2655.
Thibodeaux, C. J., Melançon, C. E. & Liu, H. (2007). *Nature (London)*, **446**, 1008–1016.
Thibodeaux, C. J., Melançon, C. E. & Liu, H. (2008). *Angew. Chem. Int. Ed.* **47**, 9814–9859.
Vidgren, J., Svensson, L. A. & Liljas, A. (1994). *Nature (London)*, **368**, 354–358.
Zhang, C., Bitto, E., Goff, R. D., Singh, S., Bingman, C. A., Griffith, B. R., Albermann, C., Phillips, G. N. Jr & Thorson, J. S. (2008). *Chem. Biol.* **15**, 842–853.
Zubieta, C., He, X.-Z., Dixon, R. A. & Noel, J. P. (2001). *Nature Struct. Mol. Biol.* **8**, 271–279.